Available online at www.sciencedirect.com
SCIENCE DIRECT®
PERGAMON
Computers and Structures 81 (2003) 2199–2217
Computers & Structures
www.elsevier.com/locate/compstruc

Dynamic behavior of a tensegrity system subjected to follower wind loading

Massimiliano Lazzari [a], Renato V. Vitaliani [a,*], Massimo Majowiecki [b], Anna V. Saetta [b]

[a] Department of Construction and Transportation, University of Padova, via Marzolo 9, Padova 35131, Italy
[b] Department of Architectural Construction, Tolentini 191, IUAV, Venice 30135, Italy

Received 14 October 2002; accepted 19 June 2003

Abstract

The aim of this paper is to present a possible develop-line for the study of large lightweight roof structures by non-linear geometric analysis, under the dynamic effects of the turbulent action of the wind, that can be applied into the classical engineering applications. In particular the paper deals with the study of tensegrity systems, that can be defined as pattern that results when push (struts) and pull (tendons) have a win–win relationship with each other. The pull is continuous and the push is discontinuous. The continuous pull is balanced by the discontinuous push producing an integrity of tension–compression. Static and dynamic analyses of the wind action effects on one example of such tensegrity system, i.e. the roof over the La Plata stadium, Argentina, have been performed by using the geometrically non-linear FE procedure named "Loki". The wind loads are simulated as deformation-dependent forces. Both experimental data and numerical results available from the roof designers, have permitted to control the reliability of the proposed mathematical model.

Keywords: Wind load; Cable-suspended structures; Geometrical non-linearity; Finite element; Dynamic analysis; Follower load

1. Introduction

A structure immersed in a given flow field, e.g. wind flux, is subjected to aerodynamic forces dependent on time and the methods of structural dynamic have to be applied to determine the response of the structure to such an action (e.g. [1]). Furthermore, the random features of wind action make it necessary to apply the theory of random vibrations. The response depends on the characteristics associated with both the structure and the wind.

It is worth noting that wind-tunnel tests together with studies of the atmospheric winds have become more necessary in recent years, because modern construction is more sensitive to wind action, especially for lightweight structural typologies.

Structures consisting of cables or membranes may be more susceptible to wind effects. In particular, cable roof structures subjected to non-symmetrical loads [2] may exhibit greater deformations than most other structures. In double curvature roofs, the load-bearing and stiffening cables form a network, which is orthogonal in most cases. Such roofs may pose serious vibration problems, requiring the provision of additional ties and lubrication of the cable intersection.

The final application of the paper is the study of tensegrity systems. Tensegrity structure was firstly conceived by Fuller [3], who defined the notions of tensegrity as a contraction of tensional and integrity. With Snelson's work in 1948 much research work on different types of tensegrity system has been carried out during the past 60 years [4].

* Corresponding author. Tel.: +39-4-9827-5622; fax: +39-4-9827-5604.
E-mail address: rvit@caronte.dic.unipd.it (R.V. Vitaliani).

0045-7949/$ - see front matter © 2003 Elsevier Ltd. All rights reserved.
doi:10.1016/S0045-7949(03)00291-8

Before Motro presented contiguous strut configuration, the essential ideas of the definition of tensegrity could be summarized as [5]: (i) composed of compression (struts) and tension (tendons) elements, (ii) struts discontinuous while cables continuous, (iii) self-stressed equilibrium. After tensegrity's definition changed about the (ii) point as "pin-jointed".

The definition also diverges at whether a cable dome can be included within tensegrity system or not. Wang [6] considers that cable domes are an extensive application of the tensegrity concept and tensegrity structures definitions can be change as (i) self-stressed equilibrium cable networks in which a continuous system of cable (tendons) are stressed against a discontinuous system of structures, (ii) composed of tensegrity simplexes.

There is also no consensus on the definition of cable domes. The main divergence lies in the different view of whether the boundary compression ring is included in the cable dome or not.

However, the most successful application of tensegrity system is the cable dome proposed by Geiger for Summer Olympic at Seoul, Korea in 1986. As an innovative, lightness dome system, it attracts a lot of attention from engineers and is widely used in large span structures, such as Rebdird Arena and the Sun Coast Dome. The largest existing dome—Georgia Dome—with an elliptical plan, was designed for the Atlanta Olympic Game in 1996 [7] by M. Levy. The Georgia dome is the first Hypar-Tensegrity Dome to built where hyperbolic paraboloid fabric panels are attached to a cable net that is stiffened by the use of tensegrity principles.

The aim of this paper is to present a possible developline for the study of such large roof structures by non-linear geometric analysis that can be applied into the classical engineering applications.

It is worth noting that the development of a non-linear static as well as dynamic analysis is a minimum requirements from the viewpoint of engineering practice, since the hypothesis of geometrical non-linear response are necessary to capture the real mechanical behavior of the tensegrity structures, indispensable in the design phase of such a construction. In the cases of standard constructions, the load parameter about both wind and snow conditions can be derived from literature (e.g. basing on national standard, collection of wind tunnel tests, books, similar constructions in similar place). On the other end, in the cases of particular construction of a certain importance (e.g. the roof of stadium), with a non-classical well know behavior, some more numerical simulations (static, dynamic, frequency analysis) as well as tunnel wind investigations (aeroelastic, aerodynamic model under laminar or turbulent flow) are indispensable.

In the present work, the cable suspension structure at La Plata Stadium in Argentina is analyzed under the effects of wind, by using the geometrically non-linear finite element procedure (named *"Loki"* [8,9]) developed according to the total Lagrangian formulation. The wind action is described as follower loading. In particular, according to the notation introduced by Schweizerhof and Ramm [10], the case of "body-attached pressure load" is considered, where only the direction depends on the deformation within each time step.

First a static analysis is carried out to study the response of the structure under the self-weight and prestressing loads and with the wind acting in the two main directions of the roof. Then the free vibration analysis is carried out and the frequencies of the structure are analyzed.

Finally a number of analyses are performed in the time domain, since the considerable displacements involved make it unsuitable to use the frequency analysis alone. In fact, determining the structure's response in the frequency domain calls for the use of several simplifying hypotheses, i.e. linearity of mechanical behavior, low turbulence factor, and negligibility of any motion of the structure. Moreover, the effects of interactions between the loading process and the response process have to be considered for such structures.

2. Wind loading: displacement-dependent pressure loading

The correct formulation of the load field and consequently its deformation dependency can become a crucial question for the overall analysis of structures in non-linear framework. In some cases the use of the improper load definitions in the structural analysis can lead to misleading results. The finite element treatment of structures with deformation dependent loads leads to the question of linearization of the possibly non-linear load–deformation relationship, resulting in an additional left hand side term to the governing equation of motion, denoted as K^{NC}, i.e. the load stiffness matrix.

Deformation dependent loads can be caused by contact of structures with liquid or gaseous media resulting in pressure forces acting normal to the contact surfaces and forces acting tangential to the surfaces. The dependency can affect direction, magnitude and distribution of the load. In this sense it is useful to describe the load by a general deformation dependent load function $\mathbf{p}(\mathbf{u})$ which is split into two parts: a scalar function p giving the magnitude of the load and a unit direction vector $\mathbf{d}$ describing the direction of the load.

$$\mathbf{p}(\mathbf{u}) = p(\mathbf{u})\mathbf{d}(\mathbf{u}) \tag{1}$$

By considering the load as depending on the deformation fields, the pressure ${}^{m}p_i$, in the current configuration m, can be written as:

$${}^{m}p_i = {}^{m}\lambda^{l} f^{k} n_i \tag{2}$$

where ${}^m\lambda$ is the load multiplier; ${}^lf = {}^lf({}^lx_j)$ represents the pressure distribution, which depends on the co-ordinates ${}^lx_j$ of the configuration l, where l is the initial configuration if $l = 0$ or the current configuration if $l = m$; ${}^kn_i$ is the unit vector perpendicular to the surface in the configuration $k = 0, m$.

Different load conditions are related to different values of the coefficients k and m, i.e.:

- $k = 0$, $l = 0$ is the classical case of dead load;
- $k = 0$, $l = m$ is a case of little practical interest;
- $k = m$ represents the most interesting cases: within the follower load class we can distinguish the *body-attached load* Fig. 1(a), characterized by $k = 0$ and $l = 0$, and the *space-attached load* Fig. 1(b), characterized by $k = 0$ and $l = m$.

Schweizerhof and Ramm [10] have introduced the notations *body-attached load* for cases where only the direction depends on the deformation **u** (i.e. gas pressure), and *space-attached load* for cases where additionally the magnitude of the load and thus its distribution over the element depends on the deformation (i.e. hydrostatic pressure).

By considering only the pressure acting on the surface A in the orthogonal direction and assuming the surface in a configuration m (${}^mA$), the external work of the pressure ${}^mp_i$ is:

$$ {}^m\delta W_{\text{ext}} = \int_{{}^mA} {}^mp_i\,\delta u_i\, d{}^ma \tag{3}$$

where u_i represents the displacement field.

2.1. Displacement-dependent stiffness

The current loaded surface can be described using a parametric formulation, in terms of the local normalized co-ordinates r and s (Fig. 2). The co-ordinates of the current surface, in configuration 2 and with reference to configuration 1, can be written as:

$$ {}^2x_i(r,s) = {}^1x_i(r,s) + u_i(r,s) \tag{4}$$

The product of the normal and reference surfaces is given by ${}^2n_i d^2a = e_{ijk}(\partial^2 x_j/\partial r)(\partial^2 x_k/\partial s)\,dr\,ds$ where $e_{ijk} = 0, -1, 1$ for an acyclic, cyclic and anticyclic sequence and the expression of the external virtual work (3) by (4) and the definition of ${}^2n_i d^2a$ omitting non-linear term becomes:

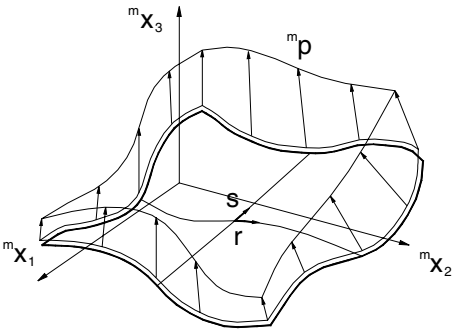

Fig. 2. Element surface loaded in normal direction.

$$ \begin{aligned} {}^2\delta W_{\text{ext}} &= e_{ijk}\,{}^2\lambda \int_r \int_s {}^lf \frac{\partial^l x_j}{\partial r}\frac{\partial^l x_k}{\partial s}\delta u_i\,dr\,ds \\ &\quad + e_{ijk}\,{}^2\lambda \int_r \int_s {}^lf \left(\frac{\partial u_j}{\partial r}\frac{\partial^l x_k}{\partial s} + \frac{\partial^l x_j}{\partial r}\frac{\partial u_k}{\partial s} \right)\delta u_i\,dr\,ds \end{aligned} \tag{5}$$

Since wind load is usually classified as a body-attached load, only such a case will be considered in the following analysis.

2.2. Body-attached load

If the load is attached to the body, the load function ${}^lf$ depends only on the initial co-ordinates, i.e. $l = 0$: ${}^0f = {}^0f({}^0x_n)$ (for *space-attached load* ${}^2f({}^2x_n) = {}^1f + (\partial^1 f/\partial^1 x_n)u_n + \cdots$, $n = 1, 2, 3$). Therefore in the expression of the external virtual work (5) the first term is independent of the current displacements and represents the usual load vector, while the second one ${}^2\delta W_{\text{ext},L}$ contains the displacement-dependent effect. Only this part denoted by L is considered below

$$ \begin{aligned} {}^2\delta W_{\text{ext},L} &= e_{ijk}\,{}^2\lambda \int_r \int_s \left(\frac{\partial u_j}{\partial r}\left(\frac{\partial^1 x_k}{\partial s}\,{}^0f\,\delta u_i \right) \right. \\ &\quad \left. + \frac{\partial u_j}{\partial s}\left(-\frac{\partial^1 x_k}{\partial r}\,{}^0f\,\delta u_i \right) \right) dr\,ds \end{aligned} \tag{6}$$

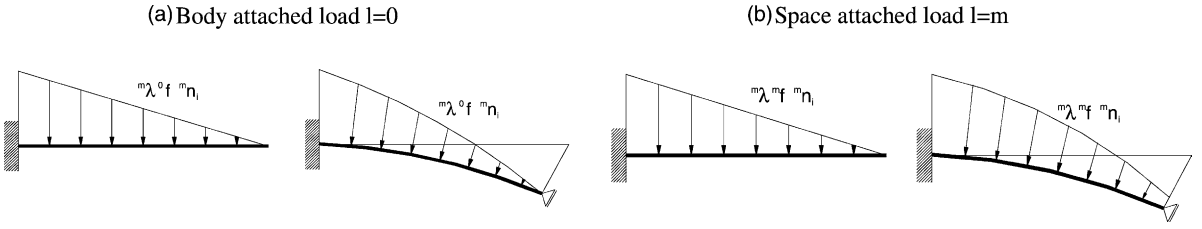

Fig. 1. Load definition [10].

Integration by parts of the load stiffness term leads to:

$$
\begin{aligned}
{}^2\delta W_{\mathrm{ext},L} = -e_{ijk}\,{}^2\lambda \int_r \int_s u_j \left(\frac{\partial}{\partial r}\left(\frac{\partial^1 x_k}{\partial s}\,{}^0 f \delta u_i \right) \right. \\
\left. + \frac{\partial}{\partial s}\left(- \frac{\partial^1 x_k}{\partial r}\,{}^0 f \delta u_i \right) \right) \mathrm{d}r\,\mathrm{d}s \\
+ e_{ijk}\,{}^2\lambda \int_{\partial R} u_j \frac{\partial^1 x_k}{\partial r}\,{}^0 f \delta u_i \,\mathrm{d}r \\
+ e_{ijk}\,{}^2\lambda \int_{\partial R} u_j \frac{\partial^1 x_k}{\partial s}\,{}^0 f \delta u_i \,\mathrm{d}s
\end{aligned} \tag{7}
$$

using the relation $\frac{\partial^0 f}{\partial r} = \frac{\partial^0 f}{\partial x_n}\frac{\partial x_n}{\partial r} = {}^0_0 f_{,n}\frac{\partial x_n}{\partial r}$, developing the derivatives term and adding (6) to both side of (7) we can rewrite the above equation in the following form:

$$
\begin{aligned}
{}^2\delta W_{\mathrm{ext},L} = \frac{1}{2} e_{ijk}\,{}^2\lambda \left\{ \int_r \int_s {}^0 f \left(\frac{\partial^1 x_j}{\partial r}\left(u_i \frac{\partial \delta u_k}{\partial s} + \delta u_i \frac{\partial u_k}{\partial s} \right) \right. \right. \\
\left. + \frac{\partial^1 x_k}{\partial s}\left(u_i \frac{\partial \delta u_j}{\partial r} + \delta u_i \frac{\partial u_j}{\partial r} \right) \right) \mathrm{d}r\,\mathrm{d}s \\
+ \int_r \int_s {}^0_0 f_{,n} \left(\frac{\partial^0 x_n}{\partial r}\frac{\partial^1 x_j}{\partial s} - \frac{\partial^0 x_n}{\partial s}\frac{\partial^1 x_j}{\partial r} \right) u_k \delta u_i \,\mathrm{d}r\,\mathrm{d}s \\
\left. + \int_b {}^0 f u_j \frac{\partial^1 x_k}{\partial s}\delta u_i \,\mathrm{d}s + \int_b {}^0 f \frac{\partial^1 x_j}{\partial r} u_k \delta u_i \,\mathrm{d}r \right\}
\end{aligned} \tag{8}
$$

By matrix notation $[\delta u]^{\mathrm{T}} = [\delta u_1 \ \delta u_2 \ \delta u_3]$, $[u]^{\mathrm{T}} = [u_1 \ u_2 \ u_3]$ and recalling that e_{ijk} has not zero only for six components, the (8) leads to:

$$
\begin{aligned}
{}^2\delta W_{\mathrm{ext},L} = \frac{1}{2}\,{}^2\lambda \left(\int_r \int_s [\delta u]^{\mathrm{T}} [\widehat{K}^{\mathrm{NC,I}}][u]\,\mathrm{d}r\,\mathrm{d}s \right. \\
+ \int_r \int_s [\delta u]^{\mathrm{T}} [\widehat{K}^{\mathrm{NC,II}}][u]\,\mathrm{d}r\,\mathrm{d}s \\
+ \int_b [\delta u]^{\mathrm{T}} [\widehat{K}^{\mathrm{NC,III}}][u]\,\mathrm{d}s \\
\left. + \int_b [\delta u]^{\mathrm{T}} [\widehat{K}^{\mathrm{NC,IV}}][u]\,\mathrm{d}r \right)
\end{aligned} \tag{9}
$$

where the operator matrix are:

Domain terms:

$$
[\widehat{K}^{\mathrm{NC,I}}] = \tfrac{1}{2}\,{}^2\lambda\,{}^0 f([D_r] - [D_s]), \qquad [\widehat{K}^{\mathrm{NC,II}}] = \tfrac{1}{2}\,{}^2\lambda[{}^0 f] \tag{10}
$$

$$
[D_r] = \begin{bmatrix} 0 & {}^1x_{3,s}({}_r\partial - \partial_r) & {}^1x_{2,s}(\partial_r - {}_r\,\partial) \\ {}^1x_{3,s}(\partial_r - {}_r\partial) & 0 & {}^1x_{1,s}({}_r\partial - \partial_r) \\ {}^1x_{2,s}({}_r\partial - \partial_r) & {}^1x_{1,s}(\partial_r - {}_r\partial) & 0 \end{bmatrix}
$$

$$
[D_s] = \begin{bmatrix} 0 & {}^1x_{3,r}({}_s\partial - \partial_s) & {}^1x_{2,r}(\partial_s - {}_s\partial) \\ {}^1x_{3,r}(\partial_s - {}_s\partial) & 0 & {}^1x_{1,r}({}_s\partial - \partial_s) \\ {}^1x_{2,r}({}_s\partial - \partial_s) & {}^1x_{1,r}(\partial_s - {}_s\partial) & 0 \end{bmatrix}
$$

$$
[{}^0 f] = \begin{bmatrix} 0 & \sum_{j=1}^3 {}^0_0 f_{,j}({}^0x_{j,s}\,{}^0x_{3,r} - {}^0x_{j,r}\,{}^0x_{3,s}) & -\sum_{j=1}^3 {}^0_0 f_{,j}({}^0x_{j,s}\,{}^0x_{2,r} - {}^0x_{j,r}\,{}^0x_{2,s}) \\ & 0 & \sum_{j=1}^3 {}^0_0 f_{,j}({}^0x_{j,s}\,{}^0x_{1,r} - {}^0x_{j,r}\,{}^0x_{1,s}) \\ \text{Skew-symmetric} & & 0 \end{bmatrix}
$$

Boundary terms:

$$
[\widehat{K}^{\mathrm{NC,III}}] = \tfrac{1}{2}\,{}^2\lambda\,{}^0 f[D_1], \qquad [\widehat{K}^{\mathrm{NC,IV}}] = \tfrac{1}{2}\,{}^2\lambda\,{}^0 f[D_2] \tag{11}
$$

$$
[D_1] = \begin{bmatrix} 0 & -{}^1x_{3,s} & +{}^1x_{2,s} \\ +{}^1x_{3,s} & 0 & -{}^1x_{1,s} \\ -{}^1x_{2,s} & +{}^1x_{1,s} & 0 \end{bmatrix}
$$

$$
[D_2] = \begin{bmatrix} 0 & +{}^1x_{3,r} & -{}^1x_{2,r} \\ -{}^1x_{3,r} & 0 & +{}^1x_{1,r} \\ +{}^1x_{2,r} & -{}^1x_{1,r} & 0 \end{bmatrix}
$$

where $\frac{\partial^1 x_k}{\partial s} = {}^1x_{k,s}$, $\frac{\partial^1 x_k}{\partial r} = {}^1x_{k,r}$, and $\delta u_j \frac{\partial u_k}{\partial s} - \frac{\partial \delta u_j}{\partial s} u_k = \delta u_j({}_s\partial - \partial_s)u_k$, $\delta u_j \frac{\partial u_k}{\partial r} - \frac{\partial \delta u_j}{\partial r} u_k = \delta u_j({}_r\partial - \partial_r)u_k$ and $({}_r\partial - \partial_r) = -(\partial_r - {}_r\partial)$.

Within the framework of the finite element approach, the load stiffness element matrices for body-attached load are always non-symmetrical in the boundary terms and in the domain terms for a non-uniform load [10].

It is worth noting that a displacement dependent load contributes with an un-symmetric component, i.e. the load stiffness matrix, to the tangent stiffness matrix and in general it cannot be expressed as $\mathbf{f} = \partial V/\partial \mathbf{u}$. However, it cannot be excluded that in same particular cases a load potential (V) could be defined, even in presence of a non-uniform load.

3. FEM numerical model

The geometrical non-linear analysis was carried out using a finite element code, named "Loki", developed according to the total Lagrangian formulation at the Department of Structural and Transportation Engineering of the University of Padova. The theoretical approach based on the total Lagrangian co-ordinate system offers considerable advantages, because of the constancy of the initial reference configuration and therefore the greater simplicity in implementation. The finite elements in GNL analysis of oriented bodies are studied considering the oriented body as a continuum, e.g. [11]. The finite elements employed in the analyses are isoparametric mono-dimensional (cable and truss) and bi-dimensional (membrane) elements in R3 space, with linear or parabolic interpolation function for the geometry and the displacements, e.g. [12–14]. The fundamental characteristics of these elements are given below, while the general references of FEM theory for static

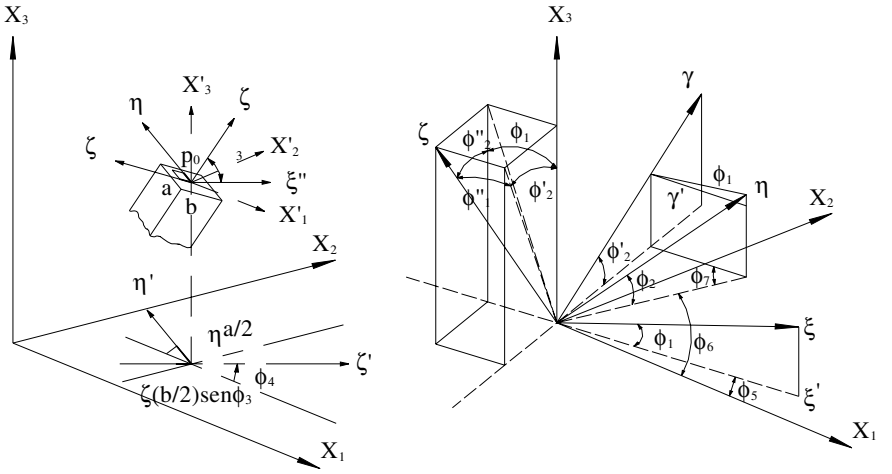

Fig. 3. Cable and membrane geometric definitions: angles between reference systems.

problems in geometric non-linearity can be found in [11,15].

Fig. 3 shows the geometry of the cable element and membrane, with the definition of the angles between the global and the intrinsic reference systems.

3.1. Geometry and displacement interpolation

The geometry of the mono-dimensional and bi-dimensional element is interpolated as a pseudo 3-D element, so that the position of a generic point of the element can be obtained as a function of the position of a point P_0 belonging to the axis or surface of the element.

For the definition of the geometry, two spaces have to be defined: the local one (ξ,η,ζ), whose base unit vectors are $\bar{l}$, $\bar{m}$ and $\bar{n}$, and the global reference one X_1, X_2 and X_3.

With such assumptions, the angles ϕ_3 and ϕ_4 between the global and the intrinsic reference systems defined in Fig. 3 are sufficient for describing the initial and current position of the element cable and truss. Four angles ϕ_1, ϕ_5 and ϕ_2, ϕ_6 are needed for identifying the local intrinsic convected frame for two-dimensional elements.

$$\text{Cable:}\quad \begin{array}{ll}\sin\phi_3(\xi)=\frac{1}{A}\frac{\partial x_3}{\partial\xi} & \cos\phi_3(\xi)=\sqrt{1-\sin^2\phi_3(\xi)}\\ \sin\phi_4(\xi)=\frac{1}{B}\frac{\partial x_3}{\partial\xi} & \cos\phi_4(\xi)=\sqrt{1-\sin^2\phi_4(\xi)}\end{array} \tag{12}$$

$$\text{Membrane:}\quad \begin{array}{ll}\operatorname{sen}\phi_1(\xi,\eta)=\frac{1}{A}\frac{\partial x_3}{\partial\xi} & \operatorname{sen}\phi_2(\xi,\eta)=\frac{1}{C}\frac{\partial x_3}{\partial\eta}\\ \operatorname{sen}\phi_5(\xi,\eta)=\frac{1}{B}\frac{\partial x_3}{\partial\xi} & \operatorname{sen}\phi_6(\xi,\eta)=\frac{1}{D}\frac{\partial x_3}{\partial\eta}\end{array} \tag{13}$$

where $A,B=\sqrt{\sum_i^M(\partial x_i/\partial\xi)^2}$ and $C,D=\sqrt{\sum_i^M(\partial x_i/\partial\eta)^2}$; for A and C the index M is equal to 3; while for B and D, the index M is equal to 2. The $\bar{m}$ and $\bar{n}$ vectors are defined as follows by simple geometrical considerations:

$$\text{Cable:}\quad \bar{m}=\begin{bmatrix}-\operatorname{sen}\phi_4\\ \cos\phi_4\\ 0\end{bmatrix},\quad \bar{n}=\begin{bmatrix}-\operatorname{sen}\phi_3\cos\phi_4\\ -\operatorname{sen}\phi_3\operatorname{sen}\phi_4\\ \cos\phi_3\end{bmatrix} \tag{14}$$

Membrane:

$$\bar{n}=\begin{bmatrix}-\cos\phi_2''\operatorname{sen}\phi_1\cos\phi_5+-\cos\phi_1''\operatorname{sen}\phi_2'\operatorname{sen}\phi_5\\ -\cos\phi_2''\operatorname{sen}\phi_1\cos\phi_5+-\cos\phi_1''\operatorname{sen}\phi_2'\operatorname{sen}\phi_5\\ \cos\phi_2''\cos\phi_1\end{bmatrix} \tag{15}$$

As a consequence the co-ordinates of a generic point P can be written as:

$$\text{Cable:}\quad x_i=\sum_k N_k(\xi)X_i^k+\frac{a}{2}\eta m_i(\xi)+\frac{b}{2}\zeta n_i(\xi) \tag{16}$$

$$\text{Membrane:}\quad x_i=\sum_k N_k(\xi,\eta)X_1^k+\frac{t}{2}\xi n_1(\xi,\eta) \tag{17}$$

where a and b are dimensions of cable section and t is the thickness of the membrane. The co-ordinate Jacobian matrix $\mathbf{J}_c$ of the transformation from (ξ,η,ζ) to (X_1,X_2,X_3) is given by:

Cable:

$$J_C=\begin{bmatrix}\sum_k N_kX_1^k+\frac{a}{2}\eta P_1(\xi,\eta)+\frac{b}{2}\zeta P_2(\xi,\eta) & \frac{a}{2}m_1 & \frac{b}{2}n_1\\ \sum_k N_kX_2^k+\frac{a}{2}\eta P_3(\xi,\eta)+\frac{b}{2}\zeta P_4(\xi,\eta) & \frac{a}{2}m_2 & \frac{b}{2}n_2\\ \sum_k N_kX_3^k+\frac{b}{2}\zeta P_5(\xi,\eta) & 0 & \frac{b}{2}n_3\end{bmatrix} \tag{18}$$

Membrane:

$$J_C = \begin{bmatrix} \sum_k \frac{\partial N_k}{\partial \xi} X_1^k + \frac{t}{2}\xi P_1(\xi,\eta) & \sum_k \frac{\partial N_k}{\partial \xi} X_1^k + \frac{t}{2}\xi P_2(\xi,\eta) & \frac{t}{2} n_1 \\ \sum_k \frac{\partial N_k}{\partial \xi} X_2^k + \frac{t}{2}\xi P_3(\xi,\eta) & \sum_k \frac{\partial N_k}{\partial \xi} X_1^k + \frac{t}{2}\xi P_4(\xi,\eta) & \frac{t}{2} n_2 \\ \sum_k \frac{\partial N_k}{\partial \xi} X_3^k + \frac{t}{2}\xi P_5(\xi,\eta) & \sum_k \frac{\partial N_k}{\partial \xi} X_1^k + \frac{t}{2}\xi P_6(\xi,\eta) & \frac{t}{2} n_3 \end{bmatrix} \tag{19}$$

where $P_i(\xi,\eta)$ are functions obtained by the derivation of $\bar{m}$ and $\bar{n}$ with respect to ξ for cable ($i = 1$–5) or by the derivation of $\bar{n}$ with respect to ξ and η for membrane ($i = 1$–6).

Therefore the deformation can be obtained by the usual relationship $\varepsilon = (J^{\mathrm{T}}J - I)/2$.

Finally the stresses can be simply evaluated from their corresponding deformations referred to the intrinsic co-ordinate system.

For the case of deformation independent loads, the tangential stiffness matrix K_{T} is simply derived as derivative of the internal forces with respect to the nodal displacements, leading to the sum of the elastic (K^E), geometric stiffness (K^L) and initial stress (K^S) matrices. In the present case, where the loads depend on the deformation, the linearization of the load operator results in an additional left hand side term, the load stiffness matrix (K^{NC}). The global stiffness matrix governing the non-linear problem is (see e.g. [16,17]):

$$K_{\mathrm{T}} = K^E + K^L + K^S - K^{\mathrm{NC}} \tag{20}$$

Large displacements and rotations, but only small strains, are assumed in the kinematics relations. A Newmark integration scheme with a full Newton–Raphson iteration technique has been employed to solve the non-linear dynamic equation.

4. La Plata stadium

The roof structure of La Plata stadium is defined as tensegrity system. Fig. 4 shows the geometry of the La Plata stadium roof, made by the same structural designer of the Georgia Dome [7]. In the following the description of such a roof is briefly reported (e.g. [18]).

"The plan of the La Plata stadium roof is obtained from the intersection of two circles with a radius of 85.62 m and centers 48 m apart. Adapting the concept to non-monotonic hoops entailed introducing an arch across the pinched waist centerline of the stadium to resist the outward thrust. Due to the presence of the kink, rigid rids were required by the arch instead of all cables.

A triangulated perimeter truss resting directly on the top of the seating berm provides resistance against both horizontal forces and gravity loads. A triangle steel trussed compression ring encircles the dome area. It is

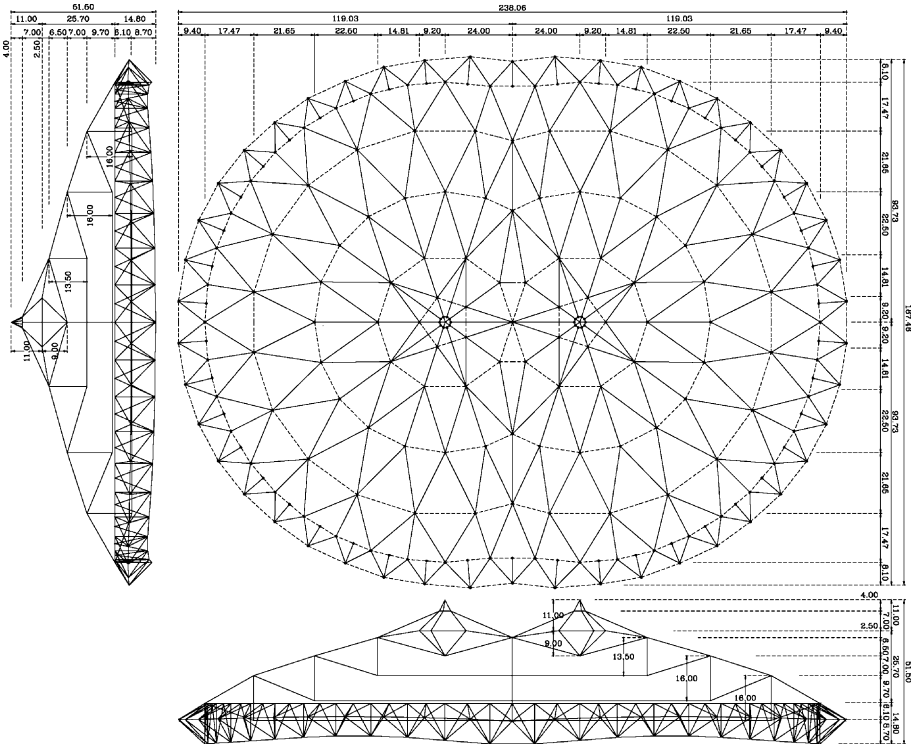

Fig. 4. Geometry of the roof structure at La Plata stadium.

about 9 m wide and 13 m high and it sits at the top of berm that forms the seating bowl for the stadium.

At the top of the compression ring posts, an inner top chord forms the spring line for the dome, which consists of the triangulated ridgnet of cables that is characteristic of the Cable Dome. A series of three tension hoops step inward and upward from the inner top chord. Radial cables hold the first of the hoops. Slopping down from the inner top chord; it supports vertical rigid posts that connect to the ridgnet. Diagonal cables angle down from that point to pick up the next tension hoop. The process repeats itself until the top of the third ring is reached. A diamond-like array of radial cables springs from the third ring to form the tent-like cupola of each peek. The cupolas permit free air flow thought an opening with a 15-m diameter in the lower level roof surface of each of two peaks. A fibber-glass membrane covers the structure.''

The analysis of structural behaviors of cables dome involves geometrical configuration finding, determination of initial stress states and the response evaluation under the external load. Since the cable dome is a geometrically flexible system, studies of cable domes should take into account non-linear features and the existence of an initial stress that gives the structural rigidity.

Such a system is fully three-dimensional and therefore benefits from the triangularization of structural elements, which enable an improvement in its load-bearing capacity.

The 3-D finite element mesh used in the analyses is composed of three main sub-structures: (a) the upper closure elements; (b) the tensegrity system and (c) the edge space-truss (Fig. 5) [19]. The cable and membrane isoparametric elements are degenerated 3-D elements, according to Φ-linear finite element theory. A synthetic description of such elements can be found in the above paragraph and in previous paper of the authors (e.g. [8]). The 3-D model of the roof includes 1168 one-dimensional two-node elements (cable and truss) and 285 four-node membrane elements. The latter are deformed so as to make two nodes coalesce.

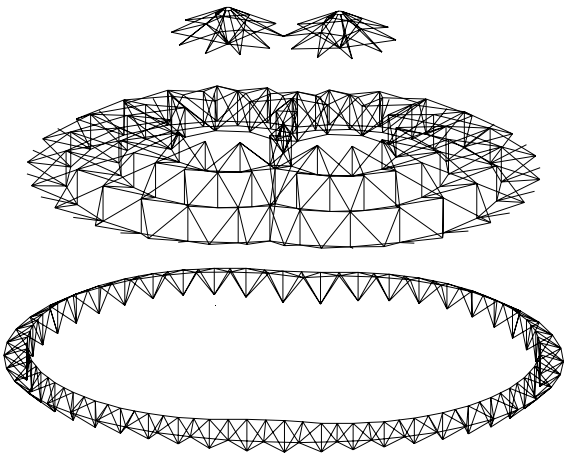

Fig. 5. Finite element model for Loki code.

4.1. Static analysis

4.1.1. ''State 0''

A cable dome needs to be pre-stressed to compensate the tendency of same cable to go slack. Instead of pre-stressing with reference to a balanced stress state, the program was left to seek a balanced configuration. This balanced configuration implies considerable deformations of the structure and the reaching of a very different stress state from the one resulting from the initial pre-stressing. In this analysis, the deformation of the edge space-truss structure coincides with a contraction due to the effect of the compression induced and this contraction causes a release of the tensegrity system and a consequent discharge of the stress in the cables and ties that form the roof. The effect of the contraction is therefore fundamental to the study of the structure as a whole. The results are compared with other two finite element codes used by the designers to perform the static loading analysis, and the LARSA program used only for the dynamic mode shape analysis. This program was been used in the past for the Georgia dome cable roof structure (e.g. [7]).

Fig. 6 shows the results of the analysis under the self-weight and pre-stressing loads, in terms of displacement contours. The maximum values of displacement in X, Y and Z directions obtained by the analysis are respectively: -0.427, -0.250 and -0.526 m corresponding to the deflection ratios $L/400$, $L/684$ and $L/323$ (where L is the minimum dimension of the suspended roof, excluding the space-truss, i.e. 171 m).

It is worth noting the good agreement of the results obtained by the present analyses with those performed by the designer of the cable roof: the BLD3D code provides maximum values of displacement $X = -0.434$ m, $Y = -0.249$ m and $Z = -0.520$; the LARSA code provides max $X = -0.447$ m, max $Y = -0.252$ m and max $Z = -0.550$. The displacement of the edge space-truss nodes laying on the X-axis in the X direction amounts to 5.39 cm, while for the corresponding points on the Y-axis the displacement is 10.95 cm.

The stress state for the first loading condition is shown in Fig. 7: it is evident that there is a high force variation between elements near each other that belong to the same level. This not homogeneous structural response behavior is more evident for the cables that compose the first and third levels of the structures and around the intersection zone of the two cables dome, while the forces in the hoop cables remain relatively constant in the entire roof. The force in some elements of the third level is very low if it is compared with other element. The behavior of the whole structure is function

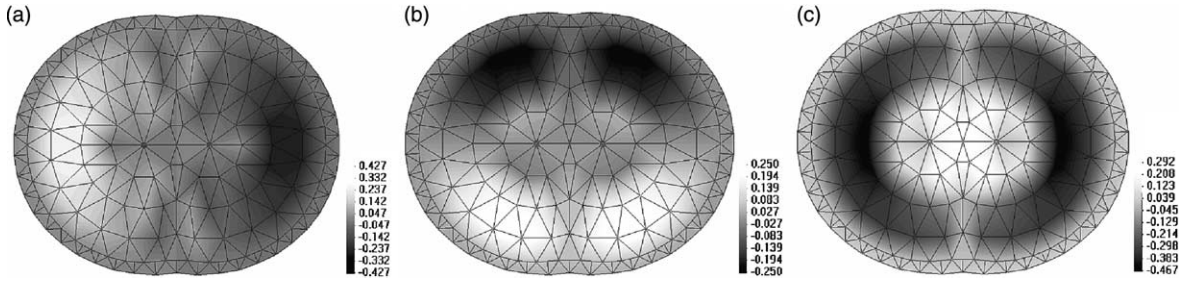

Fig. 6. Self-weight and pre-stressing loads: displacements [m] along (a) X-direction, (b) Y-direction and (c) Z-direction.

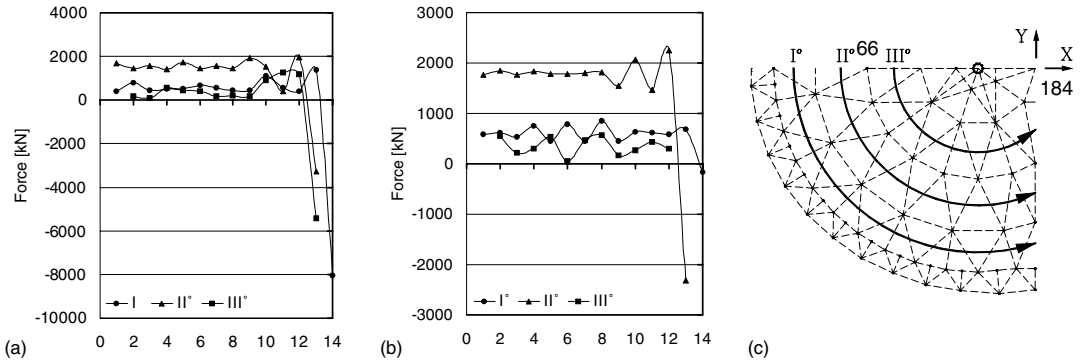

Fig. 7. Forces diagram about the up and down cable under pre-stress and dead load.

of the geometrical plan design and in particular the intersection of the two basic shape determine a singular zone that breaks the regular distribution of the cable's forces typical for circular or elliptic shape form. Introducing an arch across the pinched waist centerline of the stadium, the stiffness and the consequent behavior of the structures is not uniform for the stress and the displacement.

4.1.2. Wind load

After the equilibrium shape under pre-stress and dead load is established, the behavior of the structures is investigated under static and dynamic wind load. The static wind load is applied in 10 steps after the configuration of equilibrium for pre-stressing and self-weight has been reached.

The static analysis of the wind's action is simplified, dividing the roof into three bands in which the load acting in the direction normal to the surface takes on values of 0.50, 1.00 and 0.75 kN/m^2. The analysis is performed for the two main directions of the roof, that is with the wind acting in the X and Y directions.

The purpose of this analysis is to identify the stress and strain characteristics to use in relation to the dynamic analyses discussed later on. That is why the wind is assumed to exert an action entirely of depression over the whole surface of the roof.

The results of wind tunnel tests performed at the structural dynamics laboratory of the Federal University of Rio Grande do Sul, in Brazil (UFRGS) demonstrate that there is always a positive pressure zone, however.

The stress derived from the wind acting in the X direction (Fig. 7(a)) is characterized by the stress being cancelled in four roof cables (see Fig. 7(b)). The maximum displacements are 0.459, 0.294 and 0.715 m in the X, Y and Z directions, respectively, corresponding to the deflection ratio: 1/373, 1/582 and 1/240.

The wind load in the Y direction (Fig. 9(a)) is heavier on the structure, setting to zero the stress not only on the cables considered in the previous situation, but also in another 4 cables, as shown in Fig. 9(b). In this case the maximum displacements are 0.307, 0.342 and 0.738 m in the three directions, respectively, corresponding to the deflection ratio: 1/557, 1/500 and 1/232. Table 1 reports the comparison between the Loki response and the BLD3D response. The obtained results agree with maximum displacements obtained with other non-linear geometric code.

Observing the trends of the stresses in Figs. 8 and 9, it becomes evident that the stress response shows a non-linear behavior. In fact, the diagrams show that the re-

Table 1
Displacement comparison between Loki solution and BLD3D code

Wind direction	Displacement (m)	Node	BLD3D	Loki	Deflections
X	Max $\|x\|$	97	0.4431	0.459	1/373
	Max $\|y\|$	137	0.2815	0.294	1/582
	Max $\|z\|$	213	0.7062	0.715	1/240
Y	Max $\|x\|$	97	0.2967	0.307	1/557
	Max $\|y\|$	137	0.328	0.341	1/500
	Max $\|z\|$	183	0.7151	0.737	1/232

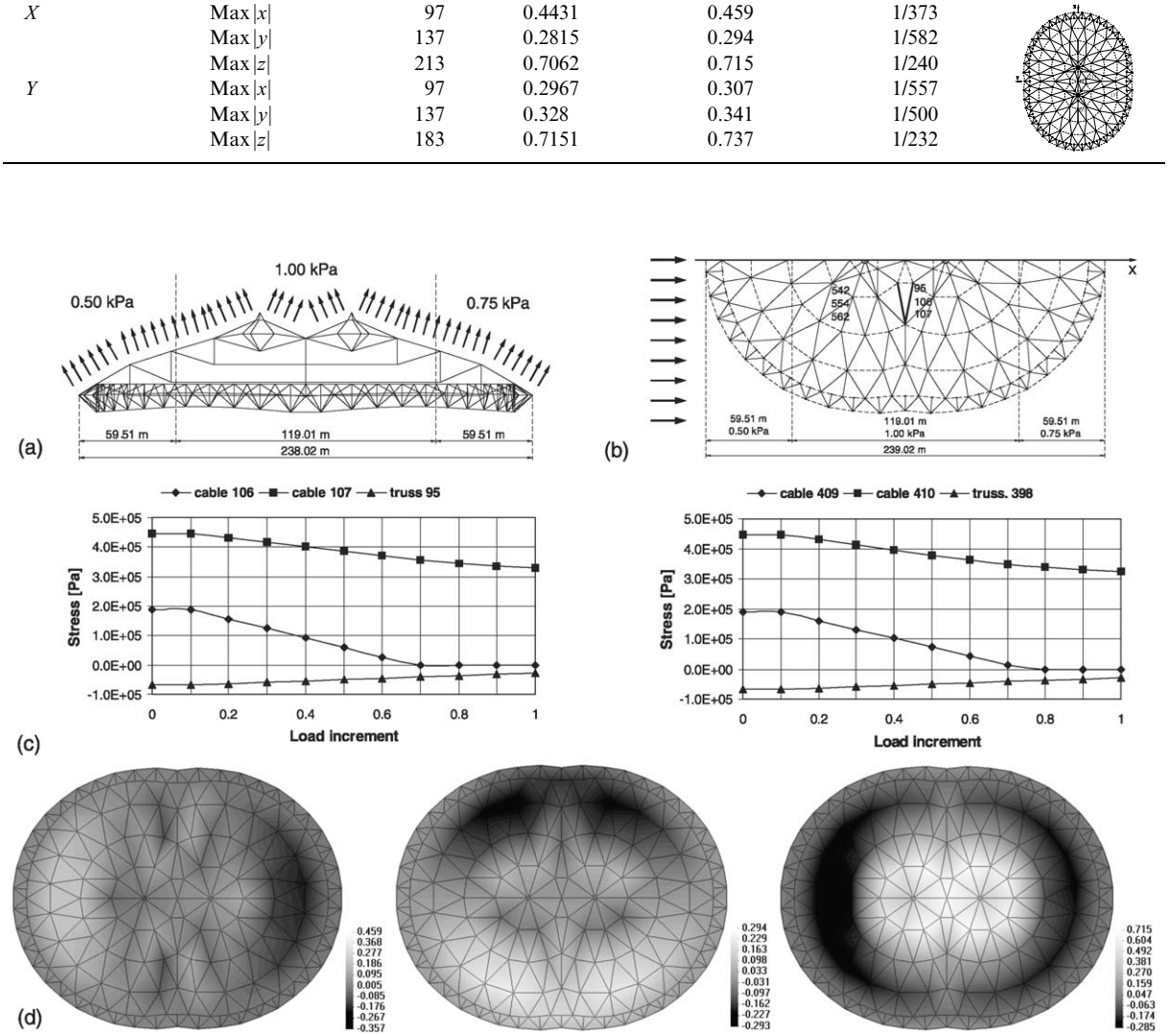

Fig. 8. Wind in X direction: (a) load configuration, (b) null cable stresses, (c) stress diagrams and (d) displacements along X-direction, Y-direction and Z-direction.

lationship between stress and increasing load is not perfectly linear. This may stem more from the fact that the attempt to establish a balanced configuration cancels the compressive stress in the cables rather than from any non-linear behavior of the structure as a whole.

The stress results (Fig. 10) show that the structure is strongly influenced by the geometry on which its design is based: it is in the area of the intersection of the two rings that the discontinuities in the stress and strain state occur. The static wind load increase the variation of the forces between elements near each other and this variation is more evident for wind load with Y direction. From Fig. 10 is clear how the rigid cables maintain a good level of pre-stress under wind load and some element increase the tension forces introduce by "state 0" for all level of the structures. While the diagonal cables reduce the force and for many cables the forces is lower than 1000 kN for the first and third level of the structure. This stress sensitive from the level is singular and describes the particular shape of the roof. Fig. 10 shows the critical cables which stress become zero.

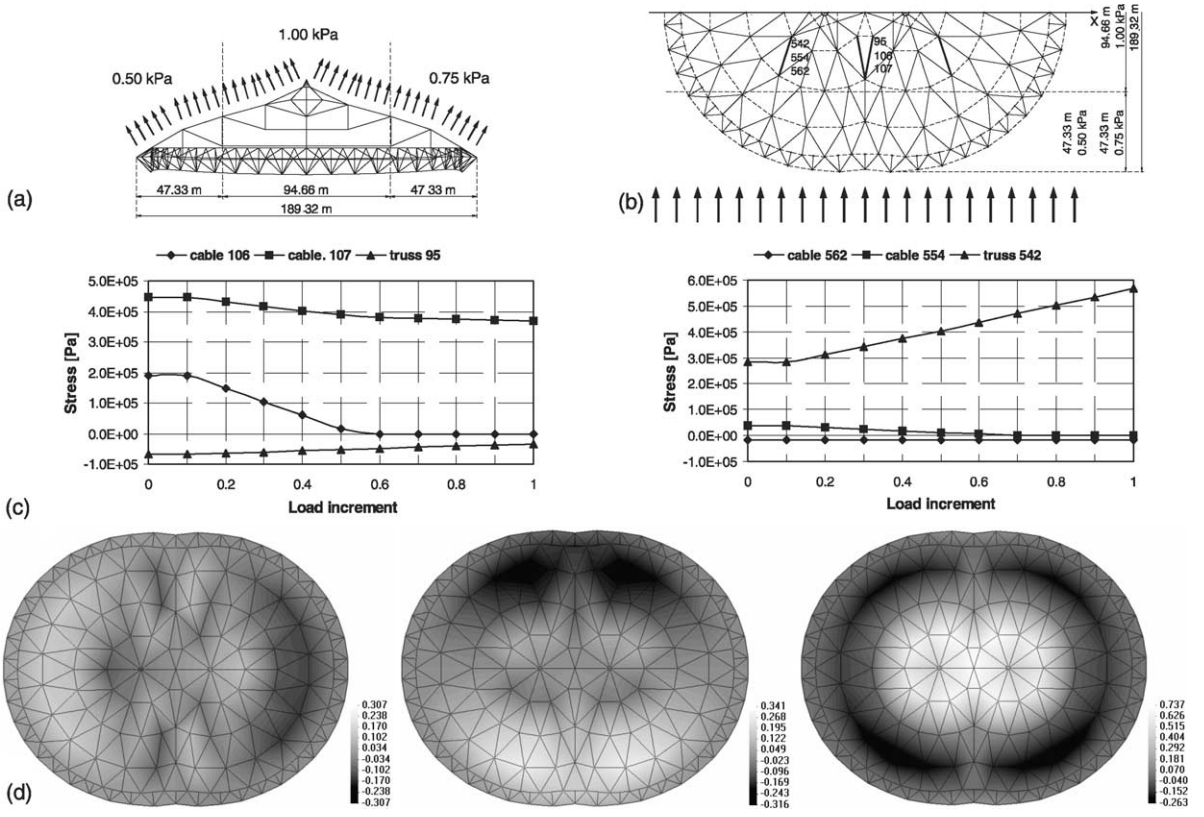

Fig. 9. Wind in Y direction: (a) load configuration, (b) null cable stresses, (c) stress diagrams and (d) displacements along X-direction, Y-direction and Z-direction.

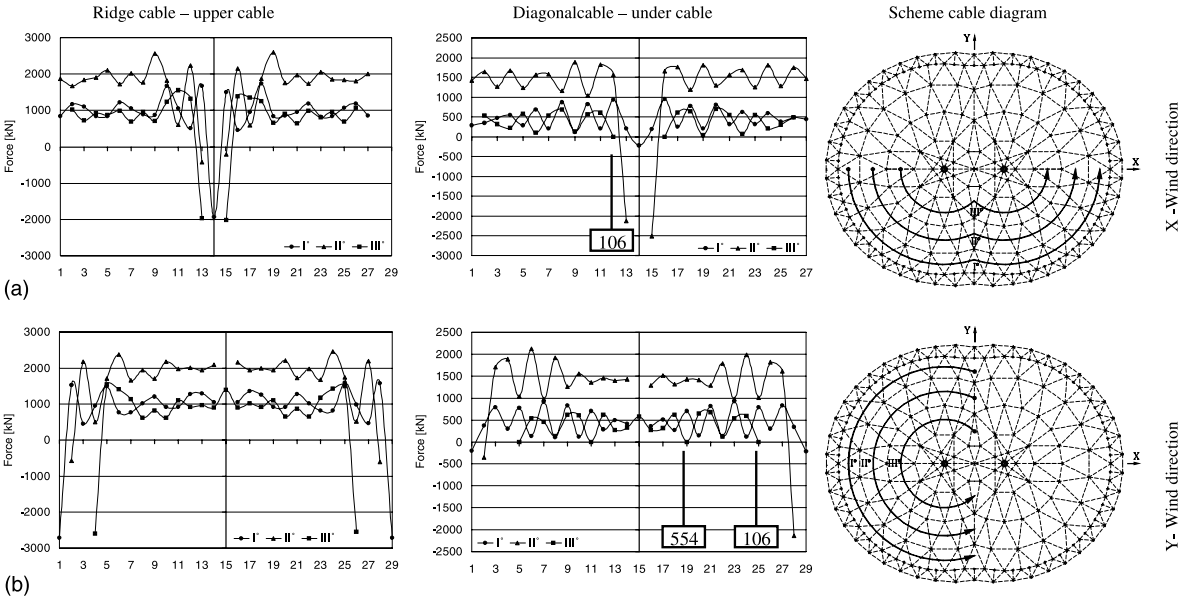

Fig. 10. Stress diagram about the up and down cable under static wind load: (a) X-direction and (b) Y-direction.

4.2. Dynamic analysis

4.2.1. Natural frequency

The frequencies of the structure were analyzed. Given the geometrically non-linear nature of the problem, the calculation is carried out with the stiffness matrix derived from the solution of problem with the pre-stressing and the self-weight of the structure. The natural frequency was obtained by solving the classic eigenvalue problem using the total stiffness matrix (20) under gravity mass matrix $[M]$. Fig. 11 shows the modal shapes of the structure.

The analysis of the frequencies and vibration modes shows that the structure behaves like an arch, since the first and third vibration modes coinciding with the first two vibration modes along direction X plane YZ and Y plane XZ are antimetric with frequencies of 1.055 and 1.443 Hz. These frequencies are taken for reference in interpreting the results obtained from the dynamic tests in the time domain through the evaluation of the power spectrum. The fundamental period is about $T_0 = 1$ s, and for the dynamic analyses in the time domain an integration step of 1/20 of T_0, i.e. 0.05 s, is used. The LARSA code provides 0.949, 1.086, 1.252 and 1.571 Hz. The first four Georgia Dome's vibration modes correspond to frequency of 0.441, 0.682, 0.716 and 0.725 Hz for the pre-stress and dead load condition. The La Plata stadium is more rigid then Georgia Dome because the frequency is about two times Georgia's frequency. The difference between the two structures is probably due to the different pre-stress state, the shape of the roofs and the presence of the up hoop cable for the La Plata Stadium. The stiffness of the whole structure, considering the very large dimension of the roof (long span 238 and 187 m), is not too much low and it is uniformly distributed. The structure is characterized by principal global stiffness and the mode and frequency derived from the interaction between the tensegrity system and the steel ring. The natural mode of the roof changes if we consider the rigid ring fix and split the structures in two parts: cable net and rigid ring. For this reason is fundamental to study the response of structure as a whole roof.

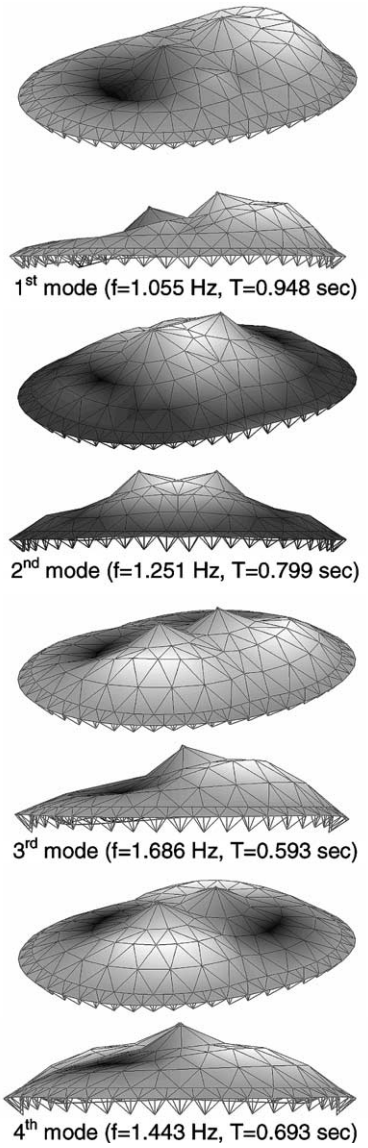

Fig. 11. First to fourth modal shapes of the cable roof.

4.2.2. Wind tunnel investigations

For the purposes of a qualitative comparison, the following paragraphs outline some of the results of the experimental study in the wind tunnel on a rigid and a reduced aero-elastic models of the roof (each constructed at 1:400 scale), performed at the structural dynamics laboratory of the Federal University of Rio Grande do Sul, in Brazil (UFRGS).

The rigid model (Fig. 12) was used to ascertain the pressure coefficients to use for the subsequent assessment of the loads due to wind. Fig. 12 also shows the pressure points, while Fig. 13 illustrates the signals measured in the tunnel on two points 23 (black line) and 34 (gray line) in terms of: time histories of the local external pressure for an incidence angle of 0°, 90°, 180° and 270°; Fourier spectral density; peak, mean and root mean square (rms) value of the pressure and C_p.

In Fig. 12 we can observe the variation of the pressure time history when the angle changes, and the two point 23 and 24 from leeward become upwind. The pressures remain negative pressures and the effect of the wind under the roof is similar to a depressor load. Near the ring in correspondence to the principal axes of the structures the pressure change the value and the sign when the wind changes the angle between its direction and the roof axes.

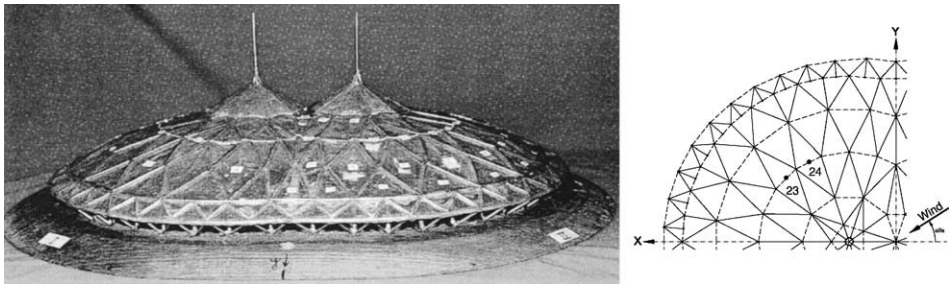

Fig. 12. Wind tunnel experiments: rigid model [20].

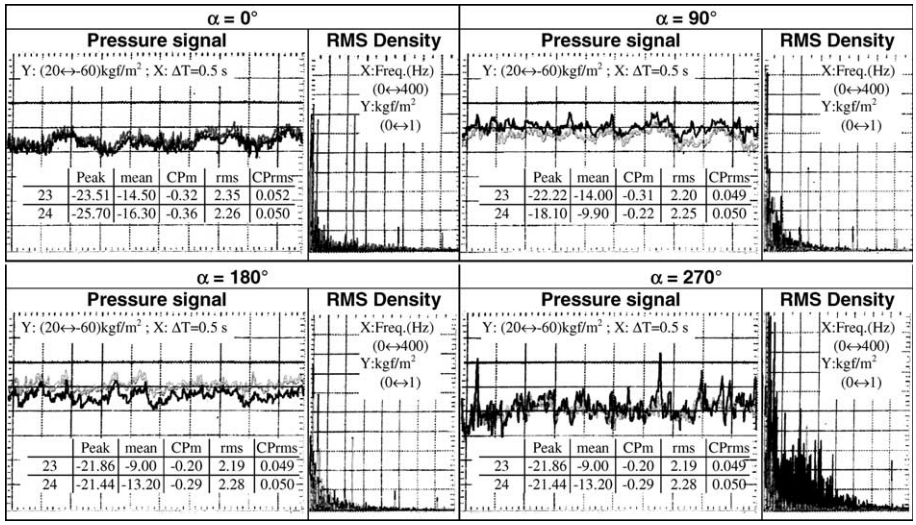

Fig. 13. Signals measured in the wind tunnel (rigid model) [20].

The comparison between the times history of the pressure carried out with reference to the center of the membrane panel and by pneumatic means of the pressure panel shown that central pressure is lower than pneumatic pressure for effect of light increase of wind static load [20].

The pressure coefficients are mapped in Fig. 14 and show that, with a wind acting in directions X and Y, there is a positive pressure in the zone where the fluid flux becomes attached to the roof, while for the rest of the roof there is only a depression. The maximum depression coefficients are found in the two upper domes.

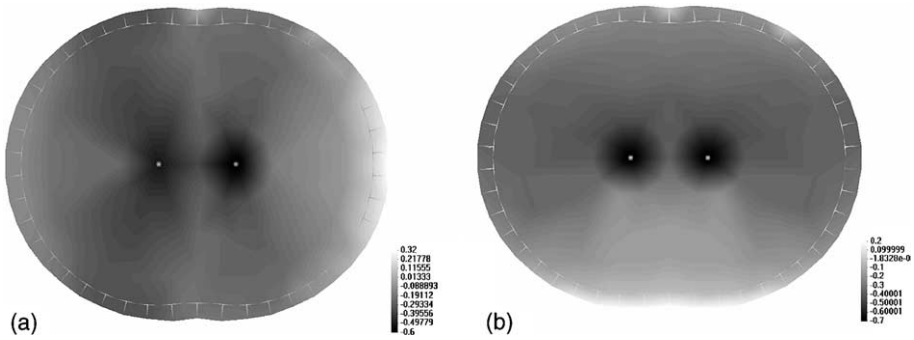

Fig. 14. Pressure coefficients along (a) X-direction and (b) Y-direction.

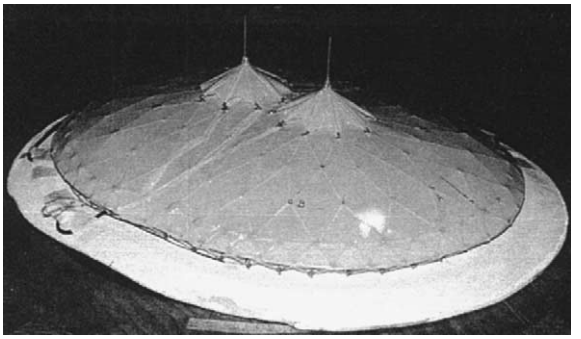

Fig. 15. Wind tunnel experiments: aero-elastic model [21].

In Fig. 14 the absolute coefficients obtained by combining the internal and external C_p coefficients are mapped.

The second model used in the experimental tests, i.e. the reduced aero-elastic model (Fig. 15) was tested in the wind tunnel with a wind coming to bear at 0°, 45° and 90° and using increasing velocities, so that the dynamic pressure was about 1/4, 1/2, 3/4 and the whole of the maximum pressure obtainable in the tunnel. The mechanical characteristics of the reduced aero-elastic model have been calibrated according to the free vibration modes calculated with the theoretical model carried out by engineer designer [21]. The element section and material used for the aero-elastic model are chosen to aim the same shapes modes between the theoretical global model of the structures and ones of the theoretical reduce model. The check of the real frequency of the aero-elastic model is carried out by the free vibration of the model under impulsive load. In this way the stiffness and damping of the aero-elastic model is tarred for realistic simulation of the structures.

The most important parameter assumed as basic geometric dimension for reduced aero-elastic model is the integral length scale (that is a measure of the linear extent of the gust in wind direction) about 100 m.

The recordings of the changes in deformations and accelerations are shown in Fig. 16, all for $\alpha = 0$. The standard deviation of the fluctuating component, for both deformation and acceleration, increases with the increasing test wind speed, bringing the dynamic amplification down towards an asymptotic value. Vibration of the structure is attributed to whirling motion originating on the edge of the roof or on the external compression ring.

The measure of the dynamic response from the structure submitted to the fluid–structure iterative effect depends on the damping and stiffness coefficient matrices of the structures modified by the iteration matrix, whose coefficients depend on the wind velocity. The system can become unstable when the basic matrices become not positive for effect of the increase wind velocity.

The reduced aero-elastic model allows for the aero-elastic stability control of the structural system. The results of the tests carried out by LDEC show the significant contribution of the stabilizing effect of the aero-elastic damping on the lightweight highly deformable structures response. The structure tested into wind tunnel does not show any effect of aero-elastic instability until the maximum velocity used into the wind tunnel.

4.2.3. Time domain simulation

Non-linear dynamic analysis in the time domain calls for the generation of a sample temporal set of wind pressure over the structure. The structure is characterized by medium-high level of structural stiffness if we compare the frequency and static displacement of the

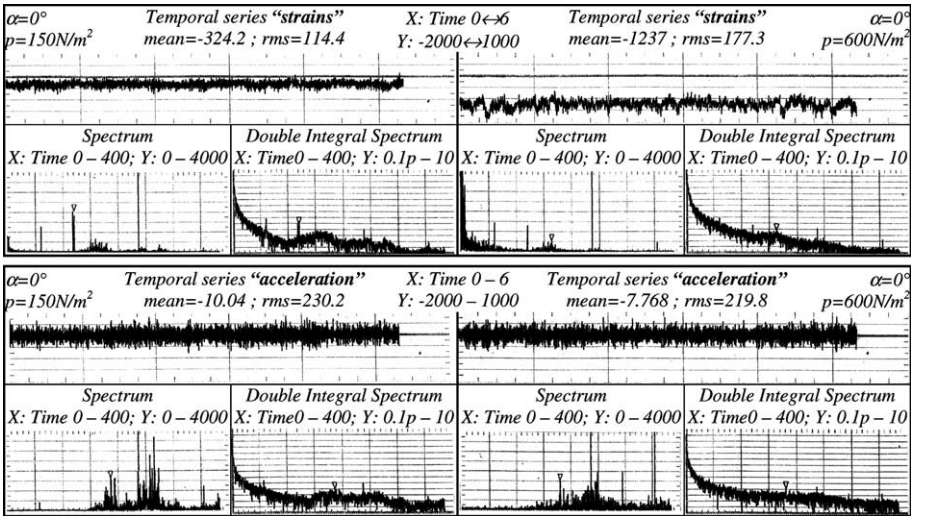

Fig. 16. Signals measured in the wind tunnel (aero-elastic model) [21].

structures with other large cable roof. For above observation we can assume in the next simulation the hypothesis of not interaction between wind force fluctuation and the structures. In this case quasi-static formulation can be assumed so we consider the coefficient of pressure constant and not function of the structural motion. By quasi-static theory the simulation of the wind pressure become the simulation of the wind velocity defined by means of the matrix of the cross-spectra that describe the stochastic component of the wind field.

This hypothesis can be considered acceptable because the structures is characterized by a local high non-linear geometric behavior but the global stiffness is enough high that the deformed structures is not far from the "state 0" configuration.

In the next analysis we do not consider the effect of the internal volume, as a restrain of the structure, because this effect can be consider not influent for the response of the system. The open area around the foot of the structure, still truss ring, permitted a high exchange of flow and a consequent low level of internal pressure.

The influence and the importance of the fluid–structure interaction effects, previously considered by the authors for membrane roofs showing very large displacement (e.g. [22]) are considered to be not essential for the response of the actual stiffer structural system. The aim of the paper, where we want present a possible develop-line for the study of large roof structures that can be applied into the classical engineering applications, included the hypotheses considered acceptable for the actual case.

Progress in computer performances now allows for simulation of a significant number of complicated real phenomena in an accurate and realistic manner. The generation of artificial samples of random data is a modern way to deal with uncertainties in variables of structural behaviors. Furthermore, it represents the most general approach, given that such numerically simulated processes must have the same statistical proprieties as the corresponding real quantities [23].

The wind structure at a given point M, is traditionally represented by assigning the vectoral temporal law of speed $\mathbf{V}(M;t)$. In most cases of practical engineering interest, the lateral and the vertical components of turbulence play a secondary role. In this situation the instantaneous velocity may be described as, e.g. [24]:

$$\mathbf{V}(M;t) = \bar{\mathbf{V}}(Z) + \mathbf{v}(M;t) \tag{21}$$

where $\bar{\mathbf{V}}(Z)$ is the mean wind speed at height z of point M of co-ordinates X, Y, Z, which produces static structural effects only, and fluctuating term $\mathbf{v}(M;t)$ which is the longitudinal component of the zero mean velocity fluctuation, a random function of space M and time t, causing a dynamic effect.

In common engineering applications, turbulence is usually treated as a multidimensional stochastic stationary Gaussian process, which is characterized, in the domain of n frequencies, by its cross-correlated power spectral density $S_v(M;M';t)$. The study of this term may be simplified by assuming that the imaginary component of the cross-spectrum is negligible for the purposes of the study that is to be carried out:

$$S_v(X,Z;X',Z';n) = \sqrt{S_v(Z;n)S_v(Z';n)}\,\mathrm{Coh}(X,Z;X',Z';n) \tag{22}$$

where $S_v(Z;n)$ represents the power spectral density function of along-wind turbulence at height Z and $\mathrm{Coh}(X,Z;X',Z';n)$ represents the coherence function of longitudinal fluctuations at points $M(X,Z)$ and $M'(X',Z')$ of the plane π orthogonal to the mean wind direction y.

The mathematical model involved is based on the Akaike–Iwatani algorithm [25,26] with a low level of regression ($AR(3)$). The data generation is based on the following stochastic characteristics:

Ground roughness: $z_0 = 0.2$ m;

Reference velocity: $v_0 = 30$ m/s at an elevation of 10 m;

Spectrum:

$$\frac{nS_v(z;n)}{u_*^2} = \frac{2.21\beta^{2.5}f}{(1+3.31\beta^{1.5}f)^{5/3}} \quad \text{with } \beta = 5.53$$

Vinckery's coherence function:

$$\mathrm{Coh}(y,z;y',z';n) = \exp\left(\frac{-2n\sqrt{C_y^2(y-y')^2 + C_Z^2(z-z')^2}}{\bar{V}(z)+\bar{V}(z')}\right)$$

where $C_Y = 11.5$ and $C_Z = 11.5$ are the decay parameters. The wind is simulated assuming the Vinckery's coherence for plane orthogonal to wind directions (cross-wind) whereas the correlation of the signal in the own direction (along wind direction) is introduced by adding a delay, $\tau = [x_i/V_m(z_i) - x_j/V_m(z_j)]$ in according with Taylor's hypothesis. Taylor's hypothesis states that the turbulence is converted downstream unchanged with the mean velocity [27]. For further details of the algorithm and of how the frequency content of the generated signal is verified, refer to [9,28].

The mean wind velocity is assumed to have a logarithmic trend. The signal is generated at all the points above the roof, amounting to a total of 167 nodes (Fig. 4) and the selected signal simulation step is 0.2 s.

The 167 histories generated by the auto-regressive simulator are the velocity field in which the structure is immersed. Fig. 17 shows the map of the velocities in 4 instants where $\Delta t = 0.2$ s for a wind acting in the X

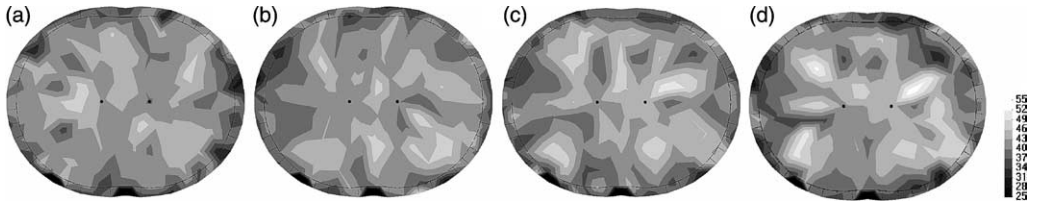

Fig. 17. Simulated wind velocity [m/s] in X direction at (a) 2 s, (b) 2.2 s, (c) 2.4 s and (d) 2.6 s.

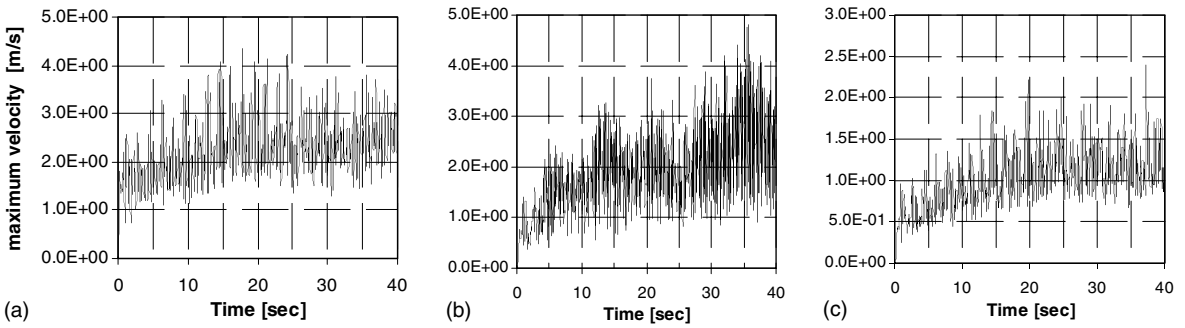

Fig. 18. Time histories of maximum structural velocity: (a) Z-direction, (b) X-direction and (c) Y-direction.

direction, illustrating the time-dependent development of the velocity field over the entire roof.

The corresponding pressure histories are assessed by means of the pressure coefficients established from the previously described wind tunnel tests on models described in the above paragraph. In the next part of the paper we refer to dynamic simulation under wind load with X along wind direction. This direction is parallel to the principal axes of the structure (Fig. 4). It is worth noting that the response of the system under other wind directions are similar to that obtained along X direction.

The dynamic analyses are performed without taking into account the effect of the relative velocity of the structure, with reference loading histories. This hypothesis is assumed to be acceptable because the structure's velocity has lowed, as it is possible to observe it in Fig. 18 were the maximum velocity for the structure in X, Y and Z directions are shown.

Fig. 19 shows the time history of total strain and total kinetic energy: the first quantity pass from zero to the static value after solution of the "state 0", pre-stress and dead load. It is worth noting that after the initial step, the dynamic simulation determine a low variation of the total strain energy. This response illustrates how the energy variation under wind load action is smaller than the level reached by pre-stress and dead load condition and the external load do not change the global behavior of the structure.

The roof is a light structures and the total kinetic energy is low and non-comparable with total strain

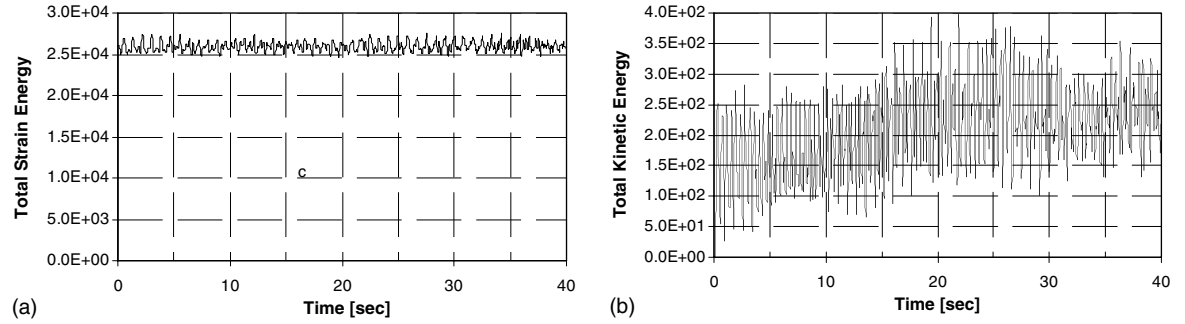

Fig. 19. Time histories of (a) total strain energy and (b) kinetic energy.

energy so the inertial forces are less important of the elastic forces.

The effect of the structural damping is not evident if we consider the diagram of the system's energy and this is due to the low structural mass of the system and the correspondent low structural damping.

The displacement's amplitude in X and Y directions are lesser than Z directions as shown in Fig. 20 for node 184 (central node of the roof, Fig. 7). The vibration is around the equilibrium state that derives from sum of "state 0" and wind static load. The mean value of X direction vibration, about -3 cm, corresponds only to the static displacement of the central point under wind load with X direction. The analysis with the power spectrum of the 184 node displacement (upper row of Fig. 21) shows that the structure submitted to a multi-correlated non-homogeneous load field has fundamental frequencies corresponding to the first frequencies assessed in the calculation of the vibration modes. In the lower row of the Fig. 21 the response of the 66 node (belonging to X axis, Fig. 7) is shown, demonstrating how the principal frequency of the response are the frequency of antimetric mode of the roof.

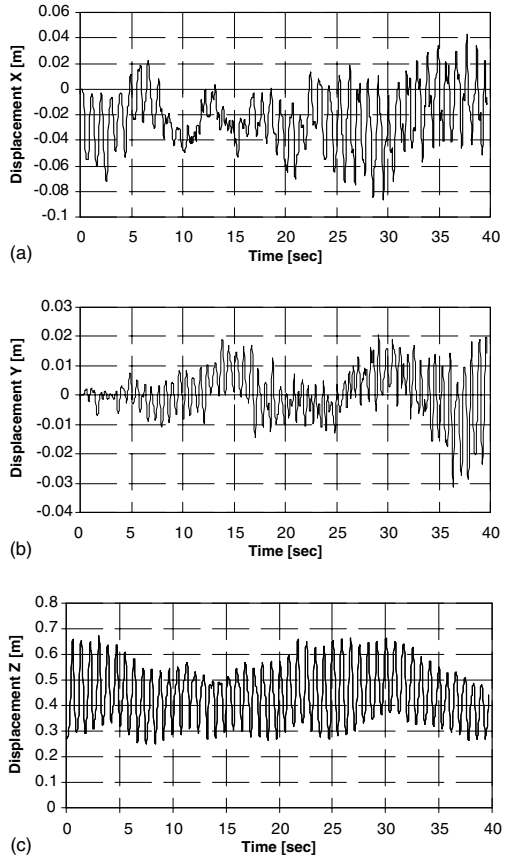

Fig. 20. History of displacements of node 184 along (a) X-direction, (b) Y-direction and (c) Z-direction.

The dynamic response of the hoop cable is characterized by a low vibration around the stress imposed by "state 0", that is a typical response of this kind of structure, and it agrees with static analysis. Instead the diagonal cable is strongly linked with the external load and the histories of the stresses, Fig. 22 reflects the behavior observed in the static analysis, with the stress in the some cables frequently becoming zero, characterizing the critical behavior of the structures. The influence of the external load is less important for the rigid cable (Fig. 22(c)) where it is evident that the effect of the wind load does not change too much the mean stress obtain by "state 0". The reason of this particular behavior is due to the type of the external load that is a depressive load.

5. Conclusion and discussion

The study of lightweight structures used for wide-span sub-horizontal roofing requires some aspects to be taken into account. In particular a minimum requirements is the development of non-linear analyses both in static and in dynamic field, the need of an accurate wind load definition, with the description of the wind's action as a force depending on the deformation, and the availability of reliable numerical procedure to deal with such constructions.

Up till now the support of wind tunnel investigations is necessary when dealing with the design phase of construction for which dynamic and aeroelastic effects are difficult to predict, like valuable tensegrity systems.

In this paper the structural response of one of such system, the La Plata Stadium roof, has been carried out by using static, frequency and dynamic analyses. Concerning the static analysis of "state 0 condition", a good agreement of the results obtained by the present analyses with those performed by the designer of the cable roof is evidenced. Similarly the static analysis of wind loading condition produce results which agree with maximum displacements obtained with other non-linear geometric code.

Then the dynamic behaviour in term of frequency analysis of the La Plata roof is compared with that obtained for other tensegrity structure (i.e. Georgia Dome) and some considerations have been carried out.

Finally the non-linear dynamic analyses of the roof have been carried out in the time domain, by assuming that there is no interaction between wind force fluctuation and the structure. The dynamic response of the roof reflects the results obtained in the static and frequency analyses, demonstrating that such a construction does not show resonance as well as instability phenomena. In particular the obtained vibration is around the equilib-

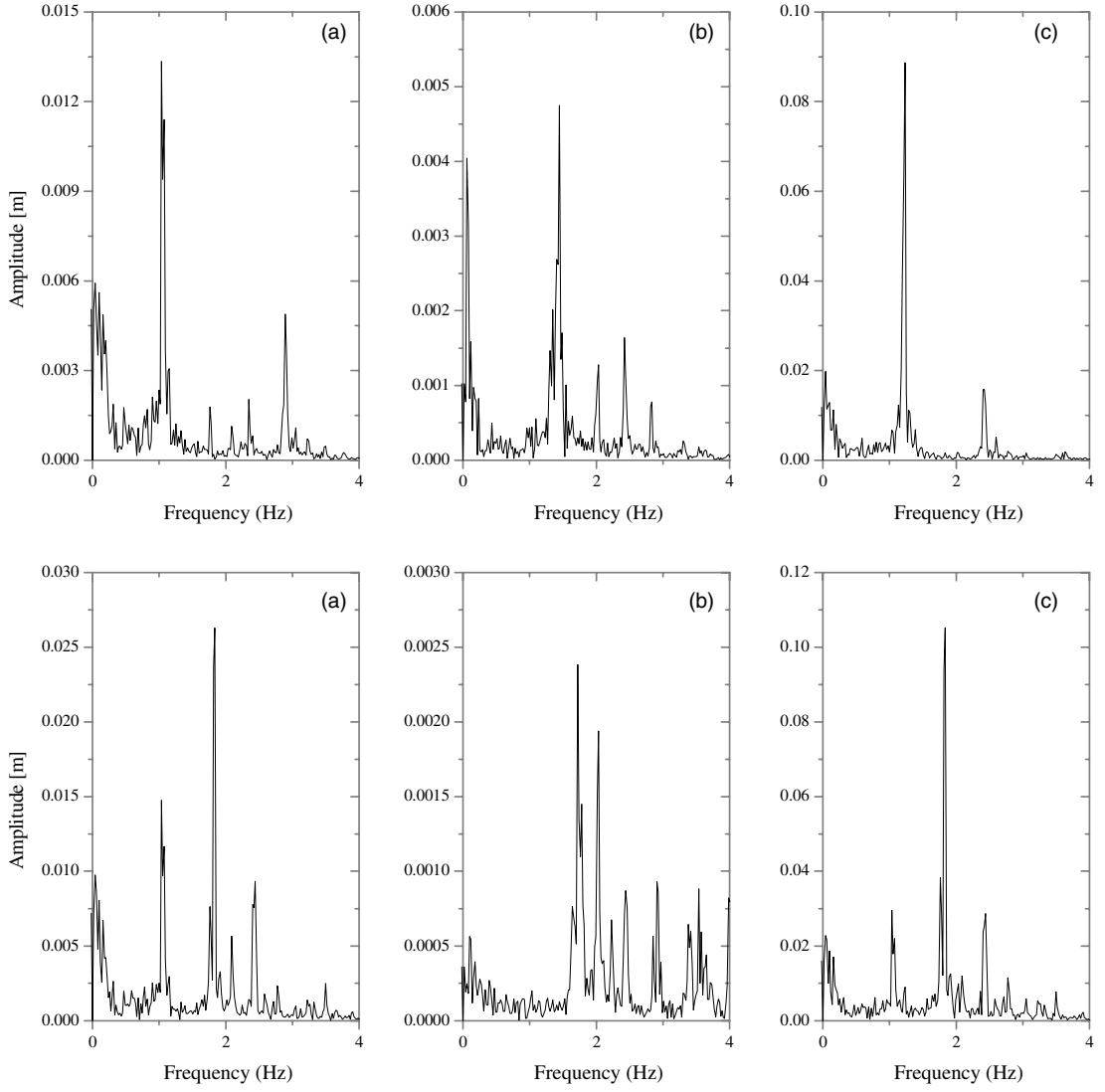

Fig. 21. Power spectral density of displacement component of node 184 (upper row) and 66 (lower row) along (a) X-direction, (b) Y-direction and (c) Z-direction.

rium state that derives from sum of "state 0" and wind static load and the structure under a multi-correlated non-homogeneous load field shows fundamental frequencies corresponding to the first frequencies assessed in the calculation of the vibration modes.

It is worth noting that the effect of the structural damping is not evident due to the low structural mass of the system and the correspondent low structural damping.

Finally the modeling approach here introduced and the results obtained in the analyses of the roof structure, assert that the prediction of the time domain response of large structures to wind loading in non-linear geometric field do not represent a prohibitive numerical and computational obstacle.

Nevertheless, further work is needed to improve the treatment of follower forces, in term of a different approach to the simulation of the load conditions. In particular a substantial improvement can be obtained by simulating directly the wind pressure and not the wind velocity from which the pressure has to be obtained by using pressure coefficients. In this way some simplified hypotheses used in the wind velocity simulation approach can be removed.

Moreover some improvement can be obtained also in the simulation of the actual stochastic characteristic of

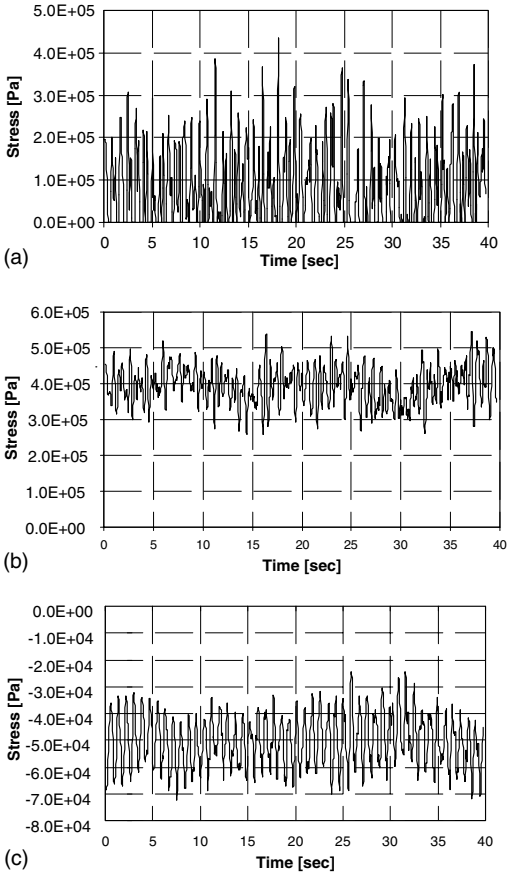

Fig. 22. History of stresses of (a) cable 106, (b) cable 107 and (c) truss 95.

wind action, which in the case of sub-horizontal structures may differ significantly from the Gaussian form.

References

[1] Simiu E, Scanlan R. Wind effects on structures. An introduction to wind engineering. John Wiley & Sons; 1996.

[2] Christiano P, Seeley GR, Stefan H. Transient wind loads on circular concave cable roof. J Struc Div ASCE 1974;100(ST11):2323–41.

[3] Fuller RB. Synergetics explorations in the geometry of thinking. London: Collier Macmillan Publishers; 1975.

[4] Yuan XF, Dong SL. Nonlinear analysis and optimum design of cable domes. Engng Struct 2002;24:965–77.

[5] Motro R. Tensegrity system: the state of the art. Int J Space Struct 1992;7(2):75–83.

[6] Wang BB. Cable-strut systems: Part I—tensegrity. J Construct Steel Res 1998;3:281–9.

[7] Castro G, Levy MP. Analysis of the Georgia Dome Cable Roof. In: Proceedings of the Eighth Conference of Computing in Civil Engineering and Geographic Information Systems Symposium, ASCE, Dallas, TX, June 7–9, 1992.

[8] Lazzari M. Geometrically Non-Linear Structures Subjected To Wind Actions, PhD thesis, University of Padua, 2002.

[9] Lazzari M, Saetta A, Vitaliani R. Non-linear dynamic analysis of cable-suspended structures subjected to wind actions. Comput Struct 2001;79/9:953–69.

[10] Schweizerhof K, Ramm E. Displacement dependent pressure loads in nonlinear finite element analyses. Comput Struct 1984;18(6):1099–114.

[11] Zienkiewicz OC, Taylor RL. The finite element method, McGraw-Hill, vol. I., 1989; vol. II, 1991.

[12] Schrefler BA, Wood RD, Odorizzi S. A total Lagrangian geometrically non-linear analysis of combined beam and cable structures. Comput Struct 1983;17(1): 115–27.

[13] Bolzon G, Schrefler BA, Vitaliani R. Finite element analysis of rubber membranes, in: Krätzig WB, Oñate E, editors. Computational Mechanics of Nonlinear Response of Shell, 1990. p. 348–77.

[14] Wood RD, Zienkiewicz OC. Geometrically non-linear finite element analysis of beam, frames, arches and axisymmetric shells. Comput Struct 1977;7:725–35.

[15] Bathe K-J. Finite element procedures in engineering analysis. Englewood Cliffs, NJ: Prentice-Hall Inc.; 1996.

[16] Vitaliani RV, Gasparini AM, Saetta AV. Finite element solution of the stability problem for nonlinear undamped and damped systems under nonconservative loading. Int J Solids Struct 1997;34(19):2497–516.

[17] Mok DP, Wall WA, Bischoff M, Ramm E. Algorithmic aspects of deformation dependent loads in non-linear static finite element analysis. Engng Comput 1999;16(5):601–18.

[18] Weidlinger Associates, http://www.wai.com/Structures/Fabric/laplata.html.

[19] Lazzari M, Majowiecki M, Saetta A, Vitaliani R. Analisi dinamica non lineare di sistemi strutturali leggeri suborizzontali soggetti all'azione del vento: lo stadio di La Plata, 5° Convegno Nazionale di Ingegneria del Vento, ANIV IN-VENTO-98, 1998 [in Italian].

[20] LDEC (Laboratorio de Dinamica Estrutural e Confiabilidade) 1/1997, UFRGS (Universiade Federal DO Rio Grande Do Sul).

[21] LDEC (Laboratorio de Dinamica Estrutural e Confiabilidade) 2/1997, UFRGS (Universiade Federal DO Rio Grande Do Sul).

[22] Lazzari M, Majowiecki M, Saetta A, Vitaliani FE. Analysis of Montreal Stadium Roof Under Variable Loading Conditions, Towards a Better Built Environment—Innovation, Sustainability, Information Technology, IABSE Symposium, Australia, September 11–13, 2002.

[23] Borri C, Zahlten W. Fully simulated non linear analysis of large structures subjected to turbulent artificial wind. Mech Struct Mach 1991;19(2):213–50.

[24] Solari G. Turbulence modeling for gust loading. J Struct Engng ASCE 1987;113(7):1550–69.

[25] Iwatani Y. Simulation of multidimensional wind fluctuations having any arbitrary power spectra and cross-spectra. J Wind Engrg 1982;11:5–18.
[26] Augusti G, Borri C, Gesella V. Simulation of wind loading and response of geometrically non-linear structures with particolar reference to large antennas. Struct Safety 1990;8:161–79.
[27] Scruton C. An introduction to wind effects on structures. Oxford University Press; 1990.
[28] Lazzari M, Majowiecki M, Saetta A, Vitaliani R. Generazione artificiale dell'azione del vento: analisi comparativa degli algoritmi di simulazione nel dominio del tempo, 5° Convegno Nazionale di Ingegneria del Vento, ANIV INVENTO-98, 1998 [in Italian].